Available online at www.sciencedirect.com
SCIENCE DIRECT®
Journal of Power Sources 151 (2005) 85–92
JOURNAL OF POWER SOURCES
www.elsevier.com/locate/jpowsour

Properties of zirconia thin layers elaborated by high voltage anodisation in view of SOFC application

Xabier Montero [a], Thierry Pauporté [a], Armelle Ringuedé [a], Rose-Noelle Vannier [b], Michel Cassir [a,*]

[a] *Laboratoire d'Electrochimie et Chimie Analytique, UMR-CNRS 7575, Ecole Nationale Supérieure de Chimie de Paris, 11, rue P. et M. Curie, 75231 Paris Cedex 05, France*
[b] *Laboratoire de Cristallochimie et Physicochimie du Solide ENSCL-BP, 59652 Villeneuve d'Ascq Cedex 108, France*

Accepted 4 February 2005
Available online 25 May 2005

Abstract

In order to adapt the anodisation technique to SOFC application, zirconium and zirconium–niobium alloys were tested in various electrolytic media and applied potentials (up to 420 V). The elaborated ZrO_2 insulating layers were characterised in situ by electrochemical impedance spectroscopy and their thicknesses were determined as ranging up to 1 μm. The effect of thermal annealing treatment of layers prepared in various experimental conditions was investigated by X-ray diffraction (XRD) and solid-state electrochemical impedance spectroscopy in a planar configuration. The effect of the growing conditions on significant parameters such as zirconia crystallite size, zirconia conductivity and activation energy were deduced up to 800 °C. The possibility of using the anodisation process for fuel cell devices is discussed. This study demonstrates that it surely requires the use of more efficient dopants, such as yttria.

Keywords: Anodisation; Zirconia; Nb-doped zirconia; Impedance spectroscopy; Solid oxide fuel cells

1. Introduction

Although the feasibility of solid oxide fuel cells (SOFC) has been clearly demonstrated, the present working temperature, above 800–850 °C, requires the use of expensive ceramics for the interconnection plates (i.e. $LaCrO_3$) and provokes the premature ageing process of the different components: anode, cathode and bipolar plates. The decrease in the working temperature of this electrochemical device is probably the main target in order to obtain reliable prototypes and to reach the commercial market. Nevertheless, decreasing the temperature down to 600–700 °C in order to increase SOFC lifetime conduces to an insufficient ionic conductivity of oxide ions through the electrolyte. Therefore, one of the most promising means to solve this problem is to reduce the electrolyte thickness and, consequently, to limit its ionic resistance [1]. The aim of the present work is to elaborate zirconia and doped zirconia-based thin layers by a cheap electrochemical method allowing to obtain dense and homogeneous layers: high voltage anodisation. Elaboration of zirconia by this technique has already been realised in the literature [2–9]; however, our purpose here is to optimise the zirconia synthesis parameters, to initiate the work on doped zirconia (i.e. with niobium) and analyse the electrical properties of these materials at high temperature. The basis of the method is to start from metallic zirconia and to oxidise this metal electrochemically in an appropriate electrolytic solution. Depending upon the pH of the solution, the global reaction can be written as:

$$Zr + 2H_2O \rightarrow ZrO_2 + 4H^+ + 4e^- \quad (1)$$

$$Zr + 4OH^- \rightarrow ZrO_2 + 2H_2O + 4e^- \quad (2)$$

Synthesis of zirconia and doped zirconia was realised at different experimental conditions, including: the applied

* Corresponding author. Tel.: +33 1 55426387; fax: +33 1 44276750.
E-mail address: michel-cassir@enscp.fr (M. Cassir).

0378-7753/$ – see front matter © 2005 Elsevier B.V. All rights reserved.
doi:10.1016/j.jpowsour.2005.02.086

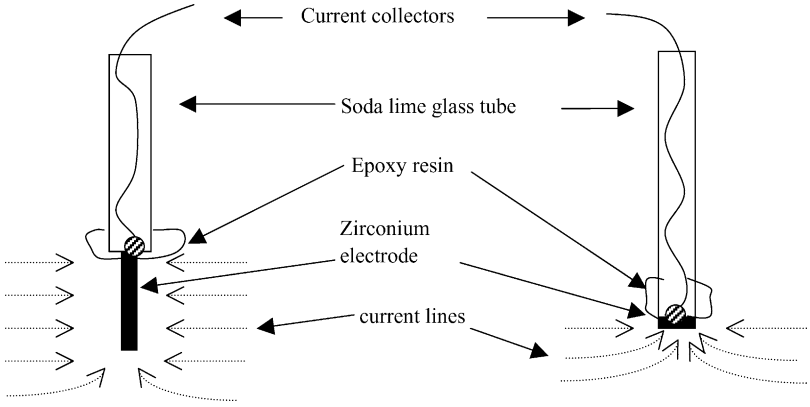

Fig. 1. View of the mounting of the zirconium rod and plate working electrodes.

potential, the electrolyte composition, pH and the matrix. The oxide formation kinetics was followed by electrochemical impedance spectroscopy. The structural and electrical properties of the mentioned materials were determined at high temperature. This study constitutes a first step towards the application of anodisation in the field of SOFC.

2. Experimental

Linear sweep voltammetry was used for the anodisation technique. Due to the insolating character of zirconia, the applied potentials must be continuously increased during the anodic coating growth and very high voltages were attained for the present investigation (above 400 V); therefore, the experimental set-up is equipped with a stabilised Keitley 2410 sourcemeter allowing to reach 1100 V and 21 mA.

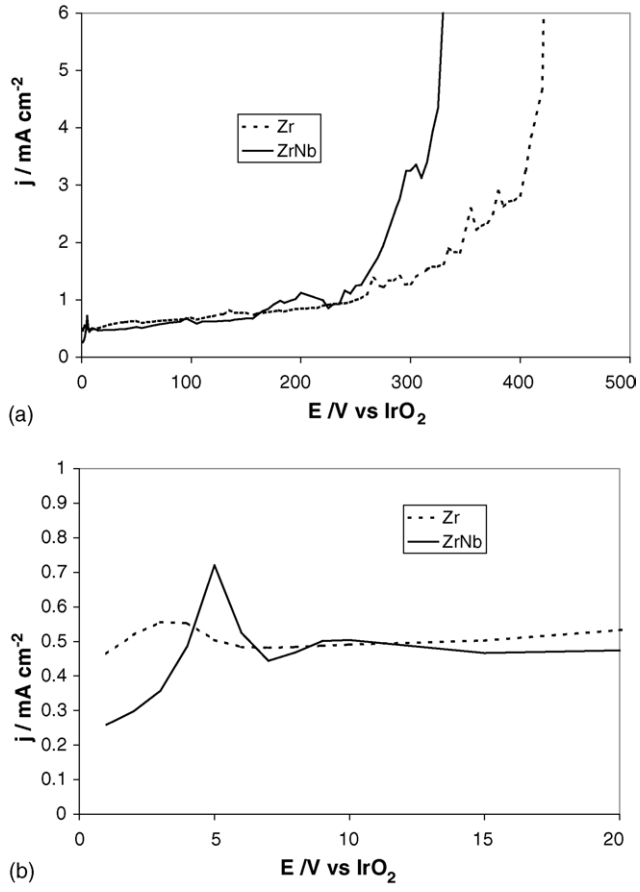

Fig. 2. (a) Voltammograms obtained at 100 mV s^{-1} in ammonium diborate 0.1 mol l^{-1}, pH 9, on Zr (99.8%) and Zr–Nb (99%–1%) plates and (b) is a detail of (a).

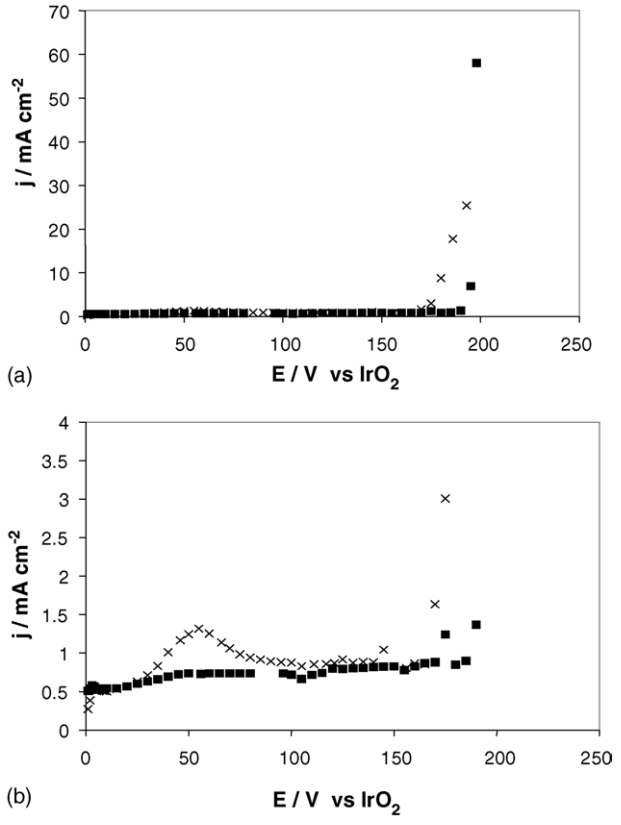

Fig. 3. (a) Zr rod (×) and Zr plate (■) voltammograms obtained at 100 mV s^{-1} in 0.1 mol l^{-1}, pH 9 sodium sulphate solution and (b) enlarged view.

Table 1
Comparison of anodic films growth speeds at 100 mV s^{-1} obtained by anodisation of zirconium or Zr–Nb alloy in different experimental conditions

Substrate	Electrolyte	Growth speed (Å s^{-1})
Zr	$(NH_4)_2B_4O_7$	2.1
Zr–Nb (1%)	$(NH_4)_2B_4O_7$	2.2–3.6
Zr	H_2SO_4	1.8–2.9
Zr	Na_2SO_4	2.4
Zr	NaOH	1.9

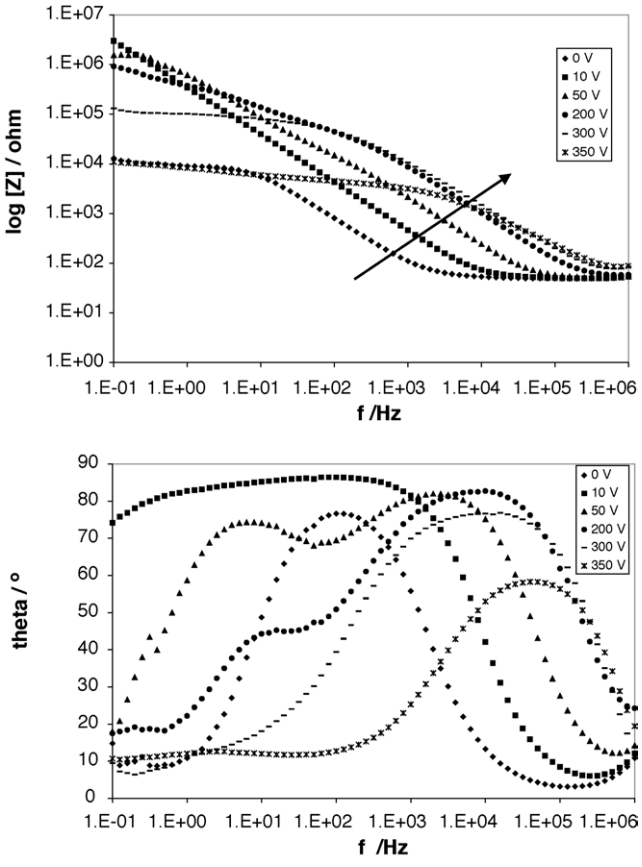

Fig. 4. Bode diagrams recorded in situ during the anodisation of Zr in 0.1 mol l^{-1}, pH 9 sodium diborate solution at 100 mV s^{-1}.

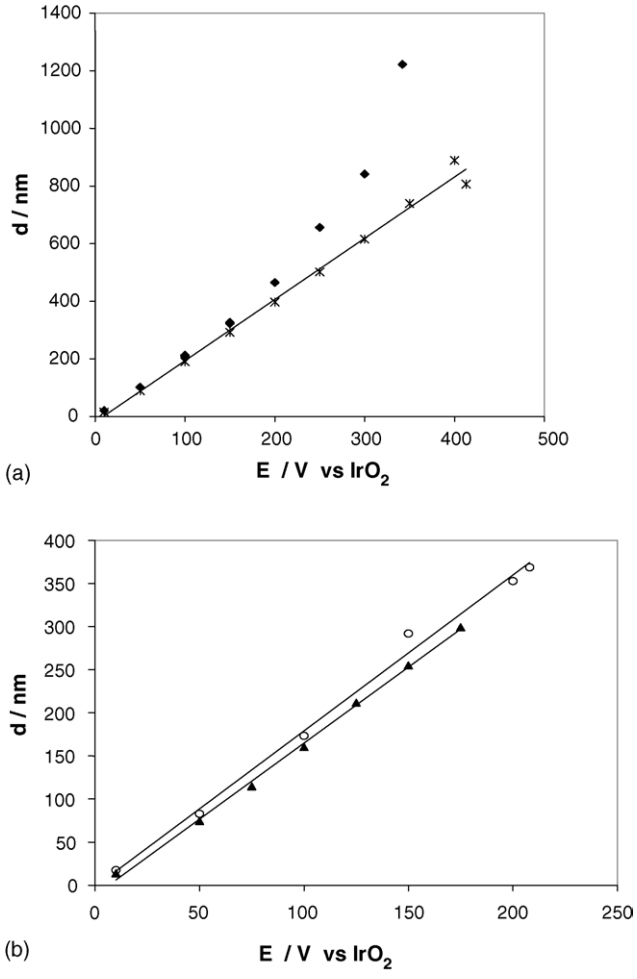

Fig. 5. Zirconia film thickness as a function of the applied voltage during anodisation. (a) Effect of zirconium alloying: zirconium (♦), Zr–1% Nb (✳) in 0.1 mol l^{-1} $(NH_4)_2B_4O_7$. (b) Effect of electrode shape: Zr plate (▲), Zr rod (◯) in 0.1 mol l^{-1} Na_2SO_4.

A two-electrode electrochemical set-up was used. The electrolysis was performed in a 100 ml glass cell. A cylindrical Ti/IrO_2 grid was used as a counter electrode. The zirconium working electrode was made from 99.8% Zr rods or plates (Goodfellows), containing as main impurities (in

Table 2
Comparison of anodisation Faradaic efficiency obtained with zirconium rods and plates in different experimental conditions

Substrate	Electrolyte	pH	Scan sweep (mV s^{-1})	Sample shape	Final potential	Faradaic efficiency (%)
Zr	$(NH_4)_2B_4O_7$	9	100	Plate	300	20
				Rod [10]	400	26
Zr	$(NH_4)_2B_4O_7$	9	33	Plate	300	23
Zr–Nb (1%)	$(NH_4)_2B_4O_7$	9	100	Plate	300	50
Zr	H_2SO_4	0, 3	100	Plate	170	77
				Rod [10]	170	43
Zr	Na_2SO_4	9	100	Plate	190	41
				Rod [10]	190	20
Zr	NaOH	13	100	Plate	290	21
				Rod [10]	290	23

ppm) Hf 2500, C 250, Fe 200, Cr 200, N 100, O 1000 and H 10. The plate diameters were 1.0 or 0.7 cm. The alloy plates, with 1 wt.% of niobium, were an industrial material product supplied by Framatome (France), with no precise list of impurities. The electrodes were mounted in a glass tube as displayed in Fig. 1.

Zirconium and alloy samples were treated similarly before the anodisation process. First of all, they were mechanically polished with SiC P400 and P1200 abrasive paper and then with a 3 μm diamond powder on metallurgical cloth. Afterwards, the samples were degreased in acetone and ethanol about 10 min each in an ultrasonic bath. Then, they were chemically etched for 2 min in a solution of HF (48%), HNO_3 (68%) and deionised water (18.2 MΩ cm) with 1:15:34 volume ratios, respectively. After this treatment, the samples had a mirror like aspect.

Different aqueous electrolytic solutions were tested: 0.5 mol l^{-1} H_2SO_4 from ultrapure 96% H_2SO_4 (Normatom from Prolabo) (pH 0.3), 0.1 mol l^{-1} Na_2SO_4 (Aldrich, reagent grade) with a pH adjusted at 9 by NaOH addition, 0.1 mol l^{-1} NaOH (Prolabo, reagent grade) (pH 13) and 0.1 mol l^{-1} ammonium biborate, $(NH_4)_2B_4O_7$, pH 9 (Sigma, reagent grade). The applied potential during anodisation will be referred to the IrO_2 electrode. During the voltage sweep, the solution was stirred vigorously with a magnetic barrel. The potential sweep was started at 0 V versus IrO_2 and performed at a constant sweep rate, classically 100 mV s^{-1}. The voltage sweep was stopped at a given potential, E_{stop}, and an impedance spectrum was recorded then at 0 V with respect to the mercurous sulphate electrode (ESM: +0.65 V/NHE), a potential close to the electrode rest potential. The voltage sweep was then continued starting at E_{stop}, stopped at a new

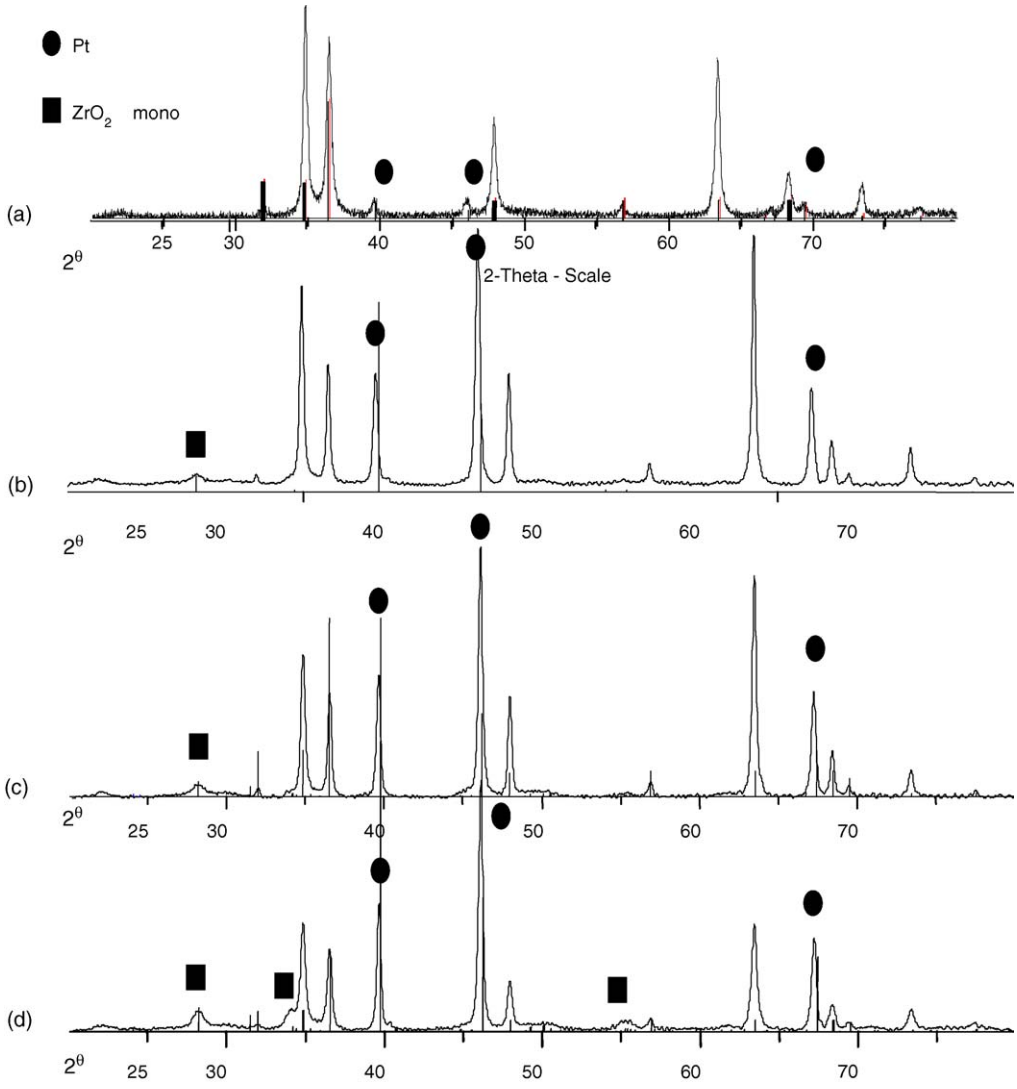

Fig. 6. XRD diagrams. (a) Pristine Zr substrate oxidised by air annealing at 800 °C during 1 h, (b) 0.6 μm thick anodic film grown on Zr in 0.1 mol l^{-1} NaOH, (c) 0.7 μm thick film grown on Zr in 0.1 M $(NH_3)_2B_4O_7$ and (d) 1.4 μm thick film on Zr–Nb (1%) in 0.1 mol l^{-1} $(NH_4)_2B_4O_7$. Peaks indexed with ZrO_2 (■) and Pt (●) (sample holder).

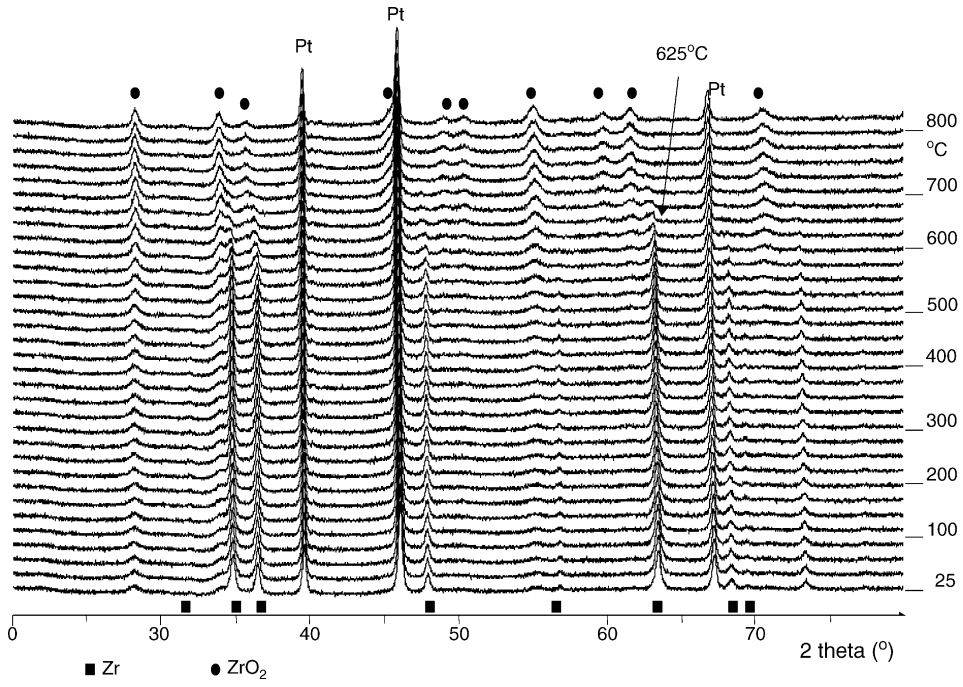

Fig. 7. XRD diagrams for increasing annealing temperature of the sample of Fig. 6d.

higher potential for impedance measurement and so on. The in situ electrochemical impedance spectroscopy (EIS) measurements were used to follow the anodic film thickness during the growth; they were realised with a EGG PAR 283 potentiostat combined with a Solartron 1255 model frequency response analyser both monitored by the Zplot-2 software from Scribner Associate. The ac signal amplitude was 30 mV and the frequency was swept from 10^6 to 10^{-1} Hz (10 points per decade).

The high temperature EIS determinations were realised with an Autolab ECO Chemie B.V. frequency analyser at the open-circuit potential. The frequency range was 10^6–10^{-2} Hz and the potential amplitude varied between 200 and 300 mV.

X-ray diffraction (XRD) analysis as a function of temperature was realised with a Siemens D5000 diffractometer equipped with a high temperature chamber Anton Paar HTK 1200, with a Cu Kα radiation ($\lambda_{K\alpha}$ = 1.5406 Å). The diffraction intensity was measured in the 20–80° (2θ) range, by steps of 0.0146°. Measurements were done between 25 and 825 °C each 25 °C, under airflow (5 l h^{-1}). The heating and cooling speeds were 0.1 and 1.0 °C s^{-1}, respectively.

3. Results and discussion

Anodisation of zirconium rod has been successfully performed and analysed in different electrolytes, such as NaOH, Na_2SO_4, H_2SO_4 and $(NH_4)_2B_4O_7$, by one of the authors [7]. For the SOFC application, we will mostly focus here on the most interesting medium, sodium diborate, which allows the growth of the thickest dense anodic films, using zirconium plate samples, which allow simple post-growth characterisation of the coatings by XRD or impedance spectroscopy.

In Fig. 2, the anodisation of a Zr and Zr–Nb (1%) alloy plates in ammonium diborate are compared. Both current density–potential curves are complex but relatively similar up to 220 V. In the case of Zr, a small current peak is observed at approximately 2–4 V, which can be attributed to oxygen evolution (proceeding from water oxidation) before metal passivation (Fig. 2b). It is followed by a slow increase in the current density with the applied potential up to 300 V. This potential domain probably corresponds to the O^{2-} migration and anodic zirconia film formation. Then, at about 400 V, the current density increases dramatically, reaching the sourcemeter saturation limit (Fig. 2a). In the case of the

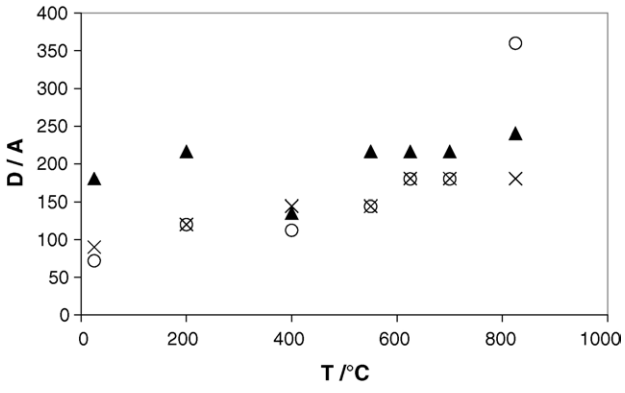

Fig. 8. Effect of annealing temperature on the crystallite grain size (in Å) as determined from the Scherrer formulae. Samples of Fig. 6b (▲) Fig. 6c (◯) and Fig. 6d (×).

alloy, the curve morphology is similar up to 220 V and then diverges, the current onset arising earlier.

In Fig. 3 are compared the anodisation of a Zr rod and a Zr plate in similar experimental conditions (sodium sulphate medium). This aspect is interesting because most of the published work in this field was done with Zr rods and it is clear that for planar SOFC applications, Zr plates are required. The peak appearing at low potentials, around 50 V, and associated to oxygen formation is more intense in the case of the Zr rod (Fig. 3b). Afterwards, the current density of the plateau is slightly higher in the case of the rod with a breakdown potential in this medium at 200 V, whereas it is of 190 V in the case of the plate. In general, we have noticed that the sourcemeter current limit is attained at a lower potential for the plates compared to the rods. The current peaks observed are smaller for the plates than for the rods; this phenomenon is more marked in the case of sulphated electrolytes (as shown in Fig. 3).

The dielectric constant and the thickness of the obtained layers were determined in situ by impedance measurements, after that the voltage sweep was stopped, according to a methodology previously described [7,8]. Fig. 4 shows the Bode diagrams obtained with a Zr–Nb (1%) alloy in ammonium diborate. It can be noted that the theta phase plot shows two relaxations after 50 V. The high frequency (HF) relaxation is observed above 100 Hz, and the low frequency (LF) relaxation below this frequency. HF relaxation is used to measure the thickness of the oxide layer formed by anodisation, according to the following relationship:

$$d = \frac{\varepsilon\varepsilon_0 S}{C_{\text{film}}} \tag{3}$$

where d is the thickness of the oxide layer, ε_0 the vacuum permittivity ($8.85 \times 10^{-14}\,\text{F cm}^{-1}$), ε the oxide dielectric constant and S is the real surface area including the roughness factor (supposing here that its value is 1). As shown in a previous work [7], the value of ε is close to 20 and varies slightly with the growing medium. C_{film} is the total oxide film capacitance, determination for which has been thoroughly described by Pauporté et al. [7]. The impedance module at HF presents a constant slope shifting towards higher frequencies when increasing the applied potential. The LF relaxation, which evolves less with the applied potential during anodisation than the HF one, can be ascribed to some porosity or defects at the sample surface.

As shown in Fig. 5, it can be observed that the film growth on zirconium (in ammonium diborate (Fig. 5a) or sodium sulphate (Fig. 5b)) is linear with respect to the applied potential. In the case of the alloy plate, linearity is not observed at potentials above 200 V where the film growth becomes significantly faster.

Table 1 summarises the principal growth speeds obtained in different experimental conditions. The growth speed is around $0.2\,\text{nm s}^{-1}$, except in H_2SO_4 (Zr plate) and $(NH_4)_2B_4O_7$ (Zr–Nb plate) where the film growth tends to increase significantly.

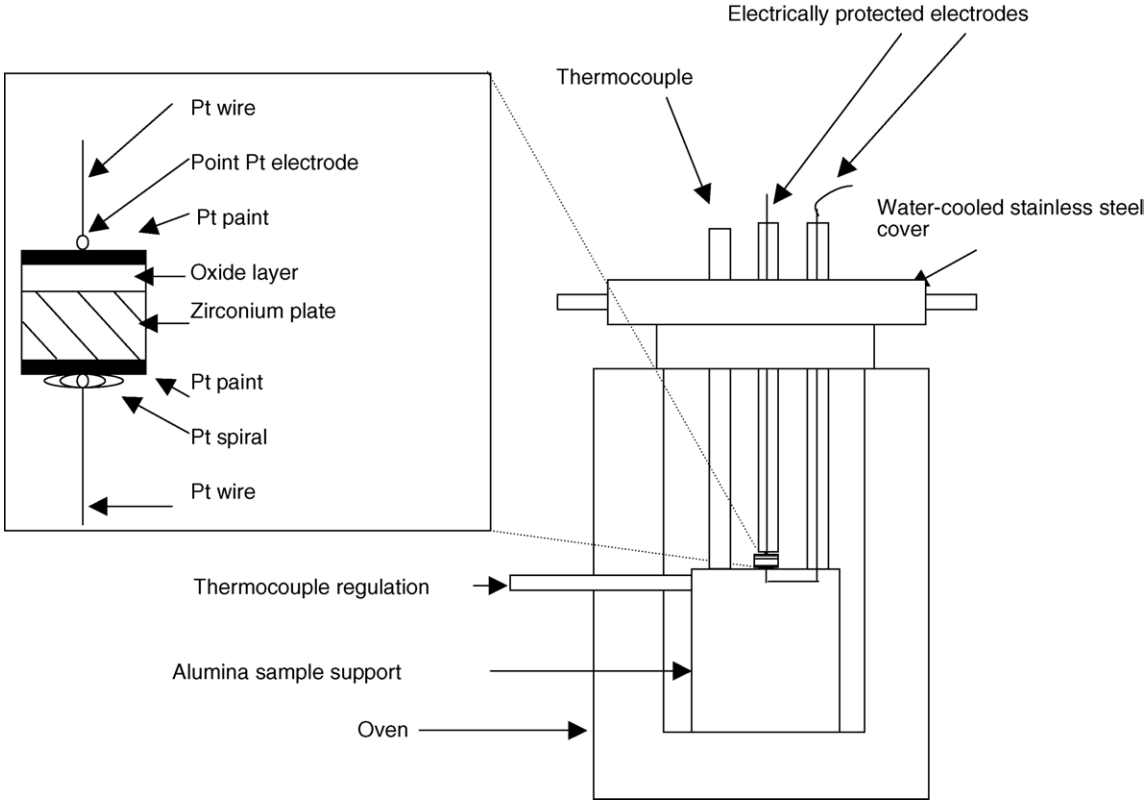

Fig. 9. Experimental set-up cell for ionic conductivity measurements.

Faradaic efficiencies related to the anodisation process are calculated from the ratio between the thickness value measured by impedance and the theoretical one, determined by the following formulae:

$$d_{\text{theoretical}} = \frac{M}{SnF\rho} \int I(t)\,\mathrm{d}t \tag{4}$$

where $I(t)$ is the current (A), t the time (s), M the zirconia molar mass (123.2 g mol^{-1}), n the electron number (4), ρ the volume density of crystallised zirconia (5.68 g cm^{-3}) and S is the electrode surface area. The global anodisation reaction is (1) in acidic and (2) in basic solutions. The main results are presented in Table 2.

In the case of the Zr plate, no clear effect of the potential scan rate was noted, in contrast to what was mentioned for the Zr rod previously [8]. Concerning the Zr–1% Nb plate, the calculated efficiency is especially high at 50% up to 300 V in spite of the non-linearity of oxide film growth (Fig. 5a). However, after 300 V, this efficiency falls down, probably due to parasitic reactions. In sulphated electrolytes (H_2SO_4 and Na_2SO_4), a significantly higher yield was obtained with Zr plate with respect to Zr rod, which could be due to parasitic reactions in the case of the rod (i.e. the peak at 50 V is relatively important for the Zr rod (Fig. 3a)). Here again, yields are higher for H_2SO_4 than Na_2SO_4 because of the non-linearity of the oxide growth in the case of the acid. For NaOH, yields are similar for both the rod and the plate.

Fig. 6 shows a comparison between the room temperature XRD spectra obtained on a pristine Zr substrate oxidised by air annealing at 800 °C during 1 h (a), anodised Zr in sodium hydroxide (b) and anodised Zr (c) and Zr–Nb alloy (d) both in ammonium diborate. It can be noted that the ZrO_2 monoclinic phase, (−1 1 1) peak at 28°, is the only visible after anodisation, showing that the layer formed by anodisation is crystallised. By comparing (c) and (d) diffractograms, one can note the influence of the substrate on the anodisation process. Only in the case of the Zr–Nb plate (Fig. 6d), two extra shoulders are visible, one at 35°, corresponding to the (2 0 0), (0 2 0) or (0 0 2) planes and the other at 55°, with a (3 0 0) or (1 2 2) orientation. Their presence can be ascribed to a better crystallisation or to the fact that the zirconia layer is thicker in the case of this substrate.

Fig. 7 represents XRD diagrams recorded with increasing annealing temperature between 25 and 825 °C in the case of the sample prepared from the Zr–Nb anodisation. At low temperature, we can mainly observe Zr and only traces of monoclinic ZrO_2. From 625 °C on, we can observe a rapid increase in the ZrO_2 peaks intensity with respect to those of Zr. At 825 °C, Zr peaks are not observed anymore. These changes are maintained when coming back to room temperature. This evolution is probably due to the recrystallisation of the formed layer. The layer formed by direct anodisation of Zr in ammonium diborate has exactly the same characteristics, which is also the case with the Zr anodisation in NaOH.

The grain size of the oxide formed by anodisation was determined by the Scherrer formulae:

$$D = \frac{0.9\lambda}{b\cos\theta} \tag{5}$$

where b is the width at half maximum of the sample peak (rad), θ the diffraction angle (rad) and λ is the X-ray wavelength (Å).

Fig. 8 represents the evolution of the grain size as a function of the temperature. The samples anodised from Zr and Zr–Nb have the same grain size at 25 °C, but their evolution with the temperature is not similar. Monoclinic ZrO_2 crystallites increase exponentially on the Zr anodised substrates and in a quasi-linear way, up to 625 °C, when the anodisation concerns the Zr–Nb alloy; afterwards, in this case, the crystal size becomes stationary. In the case of the Zr sample anodised in

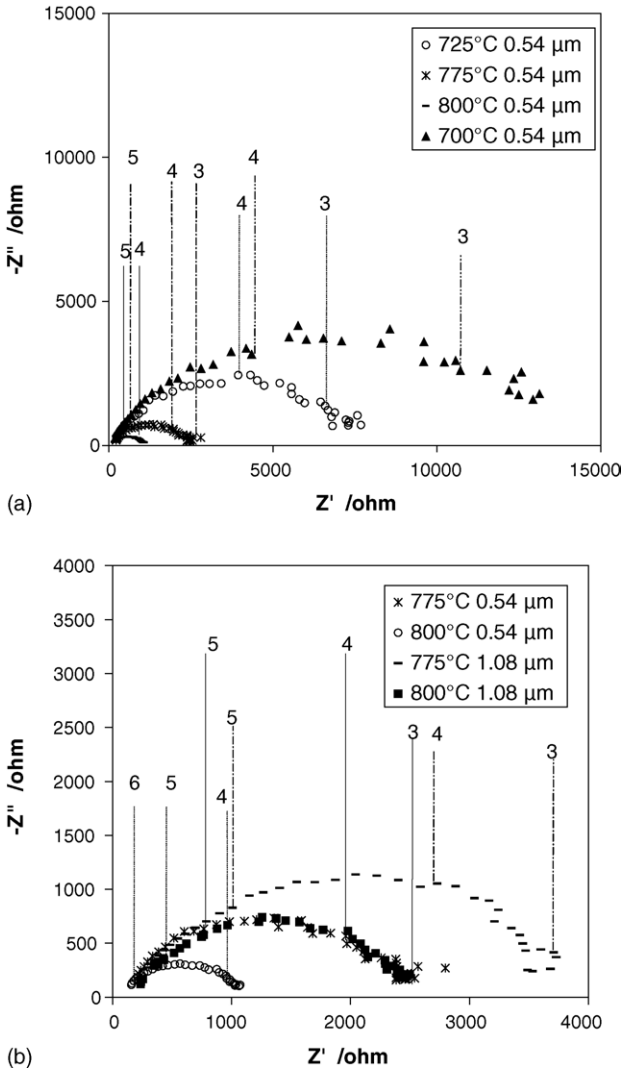

Fig. 10. Nyquist representation of the impedance spectra of a film grown on Zr in 0.1 mol l^{-1} $(NH_4)_2B_4O_7$ (S = 0.78 cm^2). (a) Effect of the temperature (0.54 μm thick film) and (b) effect of the oxide film thickness at two different temperatures.

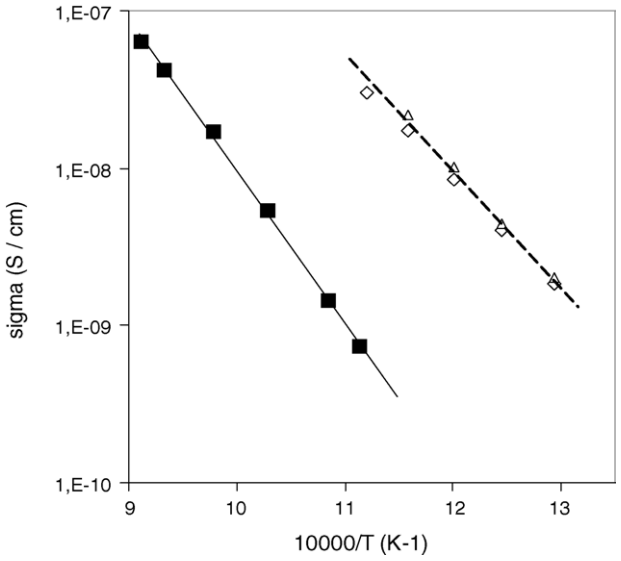

Fig. 11. Arrhenius plot of the conductivity of films grown on Zr (■) and on two Zr–Nb (◊, △) anodised in 0.1 mol l^{-1} $(NH_4)_2B_4O_7$.

NaOH, the grain size, twice bigger at low temperature, does not vary significantly with the temperature.

High temperature impedance spectroscopy allowed us to establish the samples conductivity as a function of the temperature. According to our experimental set-up, shown in Fig. 9, we have a symmetrical configuration allowing to use the following formula:

$$\sigma = \frac{l}{RS} \tag{6}$$

where σ is the ionic conductivity, R the measured resistance and l is the thickness of the oxide layer.

Fig. 10 shows the Nyquist diagrams at different temperatures (Fig. 10a) and thicknesses (Fig. 10b) in the case of the Zr plate. As expected, a regular increase in the low frequency resistance is observed with decreasing temperature or increasing thickness. Activation energies were deduced from Arrhenius plots. In the case of the Zr plate in ammonium diborate, the activation energy is 2.0 eV whatever is the thickness (1.08 or 0.54 μm), which proves the viability of anodisation as an elaboration technique. In the case of Zr–Nb alloy in the same conditions, the activation energy measured is significantly lower (1.44 eV), which could be attributed to the favourable effect of the dopant on the conductivity.

Fig. 11 shows the evolution of the conductivity as a function of the temperature for the anodised Zr (0.82 μm in thickness) and for two samples of 1.0 μm thick anodic layer on Zr–Nb sample. As expected, the conductivity of the ZrO_2 layer grown on the Zr sample is very low in comparison to what is required for the SOFC application. For the classical yttria-doped zirconia (YSZ), the conductivity is about 5×10^{-2} S cm^{-1} at 800 °C [10], instead of 4×10^{-8} S cm^{-1} for our pure anodic zirconia layer. This result is logical, knowing that non-doped ZrO_2 is not a good ionic conductor. The ionic conductivity of the Zr–Nb sample up to 625 °C is markedly higher than that of the Zr one, showing the beneficial effect of doping the film on the zirconia conductivity. It is interesting to note that this result is in good agreement with a higher corrosion speed observed on Zr–Nb compared to Zr (e.g. [11]). Therefore, the effect of film additives (dopants, ...) is very important to improve the conductivity of ZrO_2, in particular the addition of yttria in appropriate amount in the initial metal electrode may allow to attain the zirconia conductivity range required for SOFC application.

4. Conclusion

The feasibility of elaborating ZrO_2 thin layers by the anodisation of Zr or Zr–Nb (1%) plates was proven through this work. The influence of the electrolytic medium, the imposed potential and the doping effect was clearly demonstrated on the anodisation curves (current density versus potential). Different parameters were determined: oxide layer thickness, grain size and structural evolution with the temperature. High temperature impedance measurements allowed us to determine the activation energy and conductivity of the samples. In particular, all the samples analysed present a very low conductivity with respect to SOFC application. This result was expected, knowing that ZrO_2 ionic conductivity is extremely low and that the doping effect of 1% of niobium is not enough for a significant increase in the conductivity. It is obvious now, after having tested the anodisation technique on a doped sample that the next step is to anodise Zr–Y alloys in the right proportions in order to obtain the classical yttria-doped zirconia used in SOFC devices. Other dopants and oxide could also be used with the same technique.

References

[1] M. Cassir, E. Gourba, Ann. Chim. Sci. Mat. 26 (2001) 49.
[2] L. Zhang, D.D. Macdonald, E. Sikora, J. Sikora, J. Electrochem. Soc. 145 (1998) 898.
[3] J.S.L. Leach, B.R. Pearson, Electrochim. Acta 29 (1984) 1263.
[4] M.A. Abdel Rahim, A.A. Abdel Rahman, M.W. Khalil, J. Appl. Electrochem. 26 (1996) 1037.
[5] A.K. Jonsson, G.A. Niklasson, M. Veszelei, Thin Solid Films 402 (2002) 242.
[6] F. Di Quarto, S. Piazza, C. Sunseri, J. Electrochem. Soc. 131 (1984) 2901.
[7] T. Pauporté, J. Finne, J. Appl. Electrochem., submitted for publication.
[8] T. Pauporté, J. Finne, J. Schefold, D. Lincot, Surf. Coat. Technol. (2005) in press.
[9] E.M. Patrio, V.A. Macagno, J. Electroanal. Chem. 375 (1994) 203.
[10] N.Q. Minh, T. Takahashi, Science and Technology of the Ceramic Fuel Cells, Ed. Elsevier, The Netherlands, 1995.
[11] J. Schefold, D. Lincot, A. Ambard, O. Kerrec, J. Electrochem. Soc. 150 (2003) 451.